J|A|C|S ARTICLES

Published on Web 05/07/2009

Aromatic versus Antiaromatic Effect on Photophysical Properties of Conformationally Locked *trans*-Vinylene-Bridged Hexaphyrins

Min-Chul Yoon,[†] Sung Cho,[†] Masaaki Suzuki,[‡] Atsuhiro Osuka,*[,‡] and Dongho Kim*[,†]

Spectroscopy Laboratory for Functional π-Electronic Systems and Department of Chemistry, Yonsei University, Seoul 120-749, Korea, and Department of Chemistry, Graduate School of Science, Kyoto University, Sakyo-ku, Kyoto 606-8502, Japan

Received January 9, 2009; E-mail: osuka@kuchem.kyoto-u.ac.jp; dongho@yonsei.ac.kr

Abstract: We have investigated the electronic structures and energy relaxation dynamics of vinylene-bridged hexaphyrins using steady-state and time-resolved spectroscopies along with theoretical calculations in order to reveal their aromaticity-dependent electronic and magnetic properties. Ethynyl-TIPS-substituted planar and rectangular [28]hexaphyrin, regarded as a Hückel antiaromatic compound, tends to adopt a twisted Möbius aromatic topology via structural distortion in order to reduce the total internal energy, in contrast to aromatic [26]hexaphyrin, which maintains a planar conformation in solution. Spectacles-shaped vinylene-bridged [26]- and [28]hexaphyrins represent highly Hückel aromatic and antiaromatic natures, respectively, as revealed by NMR spectroscopy, giving rise to remarkable differences in NICS(0) and HOMA values and shapes of steady-state absorption and emission spectra. In particular, lifetime of the lowest singlet excited state of [28]hexaphyrin (8.6 ps) is 30 times shorter than that of the aromatic congener [26]hexaphyrin (282 ps), as measured by the femtosecond transient absorption technique. Both frontier molecular orbital analyses and vertical excitation energy calculations suggest that vinylene-bridged [28]hexaphyrin has an optically dark lowest singlet state in the NIR region, as observed in the absorption spectrum with a very low oscillator strength, which might act as a ladder state in the excited-state energy relaxation dynamics. Our findings provide further insight into the aromaticity-driven electronic properties of various porphyrinoids as well as of aromatic/antiaromatic hydrocarbon systems.

I. Introduction

Over the last century, aromaticity has been one of the most important and basic concepts in chemistry, and continuous attempts to quantify the degree of aromaticity by various indices, such as structural, energetic, reactivity, and spectroscopic criteria, has been made.[1] In parallel with this, there have been continuous efforts to synthesize and characterize new kinds of Hückel, twisted Hückel, and Möbius aromatic compounds.[2] In this context, expanded porphyrin systems have recently emerged as promising candidates to show Hückel or Möbius aromatic/antiaromatic structures because of their structural versatility and the ease of synthesizing of a set of [4*n*] and [4*n* + 2] congeners with various substituents.[3] The [4*n*]π-electronic free-base [20]isophlorin would be expected to be an antiaromatic porphyrin on the basis of Hückel's [4*n*] topology but was actually determined to be nonaromatic as a consequence of its nonplanar saddle structure.[4] On the other hand, Holten and co-workers[5] synthesized Si^{IV} tetraphenylporphyrins (SiTPPs) that can be switched between aromatic and antiaromatic congeners [SiTPP$(Cl)_2$ and SiTPP$(py)_2$, respectively] by changing the redox state of the macrocycle using axial ligation. They proposed the existence of optically dark states below the Q state, resulting in a short excited-state lifetime in antiaromatic SiTPP$(py)_2$, in marked contrast with aromatic SiTPP$(Cl)_2$.

Recently, our group has explored the photophysical properties of various expanded porphyrins, such as excited-state dynamics, nonlinear optical processes, and conformational dynamics.[3b,c,6,7] Although antiaromatic expanded porphyrins typically revealed

[†] Yonsei University.
[‡] Kyoto University.

(1) (a) Garratt, P. J. *Aromaticity*; John Wiley & Sons: New York, 1986. (b) Minkin, V. I.; Glukhovtsev, M. N.; Simkin, B. Y. *Aromaticity and Antiaromaticity: Electronic and Structural Aspects*; John Wiley & Sons: New York, 1994. (c) Cyrański, M. K. *Chem. Rev.* **2005**, *105*, 3773.
(2) (a) Jux, N. *Angew. Chem., Int. Ed.* **2008**, *47*, 2543. (b) Rzepa, H. S. *Chem. Rev.* **2005**, *105*, 3697. (c) Herges, R. *Chem. Rev.* **2006**, *106*, 4820.
(3) (a) Stepień, M.; Latos-Grażyński, L.; Sprutta, N.; Chwalisz, P.; Szterenberg, L. *Angew. Chem., Int. Ed.* **2007**, *46*, 7869. (b) Tanaka, Y.; Saito, S.; Mori, S.; Aratani, N.; Shinokubo, H.; Shibata, N.; Higuchi, Y.; Yoon, Z. S.; Kim, K. S.; Noh, S. B.; Park, J. K.; Kim, D.; Osuka, A. *Angew. Chem., Int. Ed.* **2008**, *47*, 681. (c) Park, J. K.; Yoon, Z. S.; Yoon, M.-C.; Kim, K. S.; Mori, S.; Shin, J.-Y.; Osuka, A.; Kim, D. *J. Am. Chem. Soc.* **2008**, *130*, 1824. (d) Lament, B.; Dobkowski, J.; Sessler, J. L.; Weghorn, S. J.; Waluk, J. *Chem.—Eur. J.* **1999**, *5*, 3039. (e) Lim, J. M.; Yoon, Z. S.; Shin, J.-Y.; Kim, K. S.; Yoon, M.-C.; Kim, D. *Chem. Commun.* **2009**, 261.
(4) (a) Pohl, M.; Schmickler, H.; Lex, J.; Vogel, E. *Angew. Chem., Int. Ed.* **1991**, *30*, 1693. (b) Liu, C.; Shen, D.-M.; Chen, Q.-Y. *J. Am. Chem. Soc.* **2007**, *129*, 5814.
(5) (a) Cissell, J. A.; Vaid, T. P.; Rheingold, A. L. *J. Am. Chem. Soc.* **2005**, *127*, 12212. (b) Song, H.-E.; Cissell, J. A.; Vaid, T. P.; Holten, D. *J. Phys. Chem. B* **2007**, *111*, 2138.

 10.1021/ja9000536 CCC: $40.75

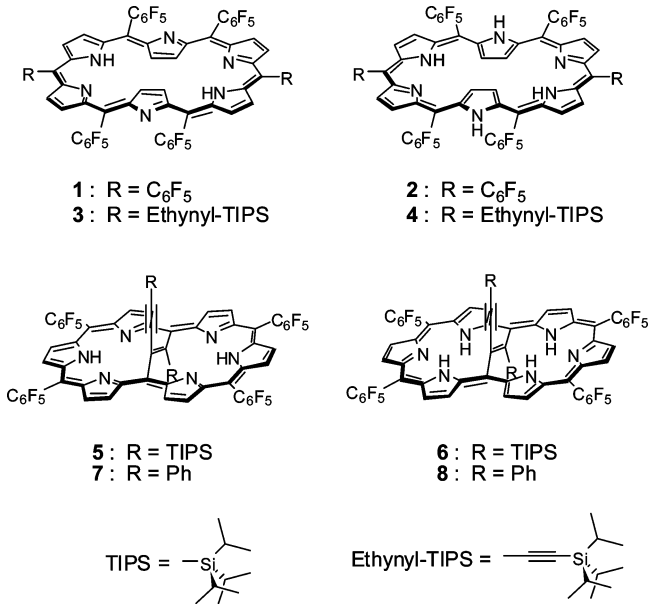

Figure 1. Molecular structures of **1**−**8** studied in this work.

shorter excited-state lifetimes than their aromatic congeners, the origin of this behavior could not be explained clearly because of the synthetic difficulty of producing purely antiaromatic molecules and the existence of various conformational isomers.[3d,6] For instance, previously reported *meso*-hexakis(pentafluorophenyl)[26]- and -[28]hexaphyrin(1.1.1.1.1.1) (**1** and **2**, Figure 1) exhibited temperature-dependent conformational dynamics leading to a difficulty in making a comparative analysis based on the difference between their electronic structures.[7] To circumvent this limitation, we introduced metal coordination to maintain a planar molecular framework, such as in bis(Au^{III})-cored [26]/[28]hexaphyrins, which are interconvertible from one to the other by a simple redox switch.[8] However, perturbations of the π electrons by the d electrons of the central metal ion as well as heavy-atom effects would be easily expected, since the transition-metal-coordinated porphyrin complexes possess partially filled d subshells. Hence, complicated electronic energy relaxation processes due to the participation of the central metal in the electronic structure of the π-conjugated macrocyclic ring should be unavoidable.[9]

In this work, we report the direct comparison of the photophysical properties of *meso*-aryl-substituted [26]- and [28]hexaphyrins that are forced to take spectacles-shaped (type-I) conformations as a result of an internal *trans*-vinylene bridge. This set of macrocycles (Figure 1) is ideally suited for use in studies aimed at revealing the influences of aromatic versus antiaromatic electronic structures on their photophysical properties without any perturbation by coordinated metals or substituents.[10] Furthermore, we have investigated the dependence of the photophysical behaviors on the hexaphyrin molecular shape (type-I versus type-II conformation, as shown in Scheme 1) by using various steady-state and time-resolved spectroscopies along with quantum-mechanical calculations. This is, to the best of our knowledge, the first study to reveal the correlation of photophysical properties with the aromatic and antiaromatic electronic properties of expanded porphyrins.

Scheme 1. Spectacles-Shaped (Type-I) and Rectangle-Shaped (Type-II) Conformations of Representative [26]Hexaphyrin(1.1.1.1.1.1) Molecules, with Their π-Electron Conjugation Pathways Marked as Thick Lines

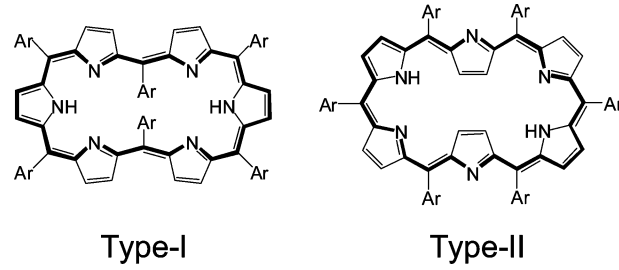

II. Experimental Section

Sample Preparation. Details concerning the synthesis, characterization, and X-ray crystallographic analysis of **3**−**8** are described elsewhere.[10] All of the reagents and solvents were of commercial reagent grade and used without further purification. ^{1}H NMR spectra were recorded on a JEOL ECA-600 spectrometer (operating at 600.17 MHz for ^{1}H) using the residual solvent in $CDCl_3$ as an internal reference for ^{1}H (δ = 7.26 ppm).

Steady-State Absorption and Fluorescence. UV−vis−NIR absorption spectra were recorded on a commercial absorption spectrometer (Varian, Cary 5000). The near-infrared (NIR) fluorescence was detected using a monochromator (Acton Research, SP2150) with a focal length of 15 cm, an attached NIR photomultiplier tube (Hamamatsu, H9170−75), and a lock-in amplifier (EG&G, 5210) combined with a mechanical chopper, after laser excitation at 442 nm from a continuous wave (CW) He−Cd laser (Melles Griot, Omnichrome 74). A quartz cell with an optical path length of 10 mm was used for all of the steady-state measurements.

Femtosecond Transient Absorption. The femtosecond time-resolved transient absorption (TA) spectrometer consisted of homemade noncollinear optical parametric amplifier (NOPA) pumped by a Ti:sapphire regenerative amplifier system (Quantronix, Integra-C) operating at a repetition rate of 1 kHz and an optical detection system.[11] The generated visible NOPA pulses that were used as pump pulses had a pulse width of ~100 fs and an average power of 1 mW in the range 480−700 nm.[12] White-light-continuum (WLC) probe pulses were generated using a 2 mm thick sapphire window on which was focused a small fraction of the fundamental 800 nm pulses that had been picked off by a quartz plate before entering the NOPA. The time delay between the pump and probe beams was carefully controlled by making the pump beam travel along a variable optical delay (Newport, ILS250). Intensities of

(6) (a) Yoon, Z. S.; Kwon, J. H.; Yoon, M.-C.; Koh, M. K.; Noh, S. B.; Sessler, J. L.; Lee, J. T.; Seidel, D.; Aguilar, A.; Shimizu, S.; Suzuki, M.; Osuka, A.; Kim, D. *J. Am. Chem. Soc.* **2006**, *128*, 14128. (b) Yoon, Z. S.; Cho, D.-G.; Kim, K. S.; Sessler, J. L.; Kim, D. *J. Am. Chem. Soc.* **2008**, *130*, 6930. (c) Yoon, M.-C.; Misra, R.; Yoon, Z. S.; Kim, K. S.; Lim, J. M.; Chandrashekar, T. K.; Kim, D. *J. Phys. Chem. B* **2008**, *112*, 6900. (d) Kwon, J. H.; Ahn, T. K.; Yoon, M.-C.; Kim, D. Y.; Koh, M. K.; Kim, D.; Furuta, H.; Suzuki, M.; Osuka, A. *J. Phys. Chem. B* **2006**, *110*, 11683.
(7) (a) Sankar, J.; et al. *J. Am. Chem. Soc.* **2008**, *130*, 13568. (b) Ahn, T. K.; Kwon, J. H.; Kim, D. Y.; Cho, D. W.; Jeong, D. H.; Kim, S. K.; Suzuki, M.; Shimizu, S.; Osuka, A.; Kim, D. *J. Am. Chem. Soc.* **2005**, *127*, 12856.
(8) Mori, S.; Kim, K. S.; Yoon, Z. S.; Noh, S. B.; Kim, D.; Osuka, A. *J. Am. Chem. Soc.* **2007**, *129*, 11344.
(9) (a) Andréasson, J.; Kodis, G.; Lin, S.; Moore, A. L.; Moore, T. A.; Gust, D.; Mårtensson, J.; Albinsson, B. *Photochem. Photobiol.* **2002**, *76*, 47. (b) Drain, C. M.; Gentemann, S.; Roberts, J. A.; Nelson, N. Y.; Medforth, C. J.; Jia, S.; Simpson, M. C.; Smith, K. M.; Fajer, J. F.; Shelnutt, J. A.; Holten, D. *J. Am. Chem. Soc.* **1998**, *120*, 3781. (c) Yoon, M.-C.; Noh, S. B.; Tsuda, A.; Nakamura, Y.; Osuka, A.; Kim, D. *J. Am. Chem. Soc.* **2007**, *129*, 10080.
(10) Suzuki, M.; Osuka, A. *J. Am. Chem. Soc.* **2007**, *129*, 464.
(11) Koide, T.; Kashiwazaki, G.; Suzuki, M.; Furukawa, K.; Yoon, M.-C.; Cho, S.; Kim, D.; Osuka, A. *Angew. Chem., Int. Ed.* **2008**, *47*, 9661.
(12) Cerullo, G.; De Silvestri, S. *Rev. Sci. Instrum.* **2003**, *74*, 1.

Table 1. Measured[a] and Calculated[b] ^{1}H NMR Peaks and NICS and HOMA Values for **3**−**6**

sample	method	chemical shift (ppm) [no. of H] inner N−H	outer N−H	inner β-H	outer β-H	TIPS-H	NICS(0) (ppm)[f]	HOMA opt (X-ray)[g]	Hückel aromaticity
3	exptl	−1.92 [2]	−	−2.23 [4]	9.37 [4] 9.91 [4]	1.51 [36] 1.58 [6]			aromatic
	calcd	−6.2 [1] −6.8 [1]	−	−3.8 to −6.6 [4]	9.9 to 10.9 [8]	1.2 to 2.5 [42]	−15.0	0.830 (0.842)	aromatic
4	exptl	3.90 [2]	8.26 [2]	2.08 [1] 2.78 [2]	7.61 [2] 7.84 [2] 7.91 [2] 8.05 [2]	0.75 [42]			nearly aromatic
4H[c]	calcd[c]	57.2 [1] 57.4 [1]	−8.3 [1] −10.0 [1]	41.3 to 44.1 [4]	−0.28 to −4.0 [8]	−1.4 to 0.60 [42]	35.2	0.670	antiaromatic
4M[d]	calcd[d]	−0.50 [1] 0.96 [1] 3.9 [1]	12.3 [1]	−2.41 [1] −4.3 [1] 4.8 [2]	8.1 to 9.2 [8]	−2.4 to 2.1 [42]	−13.0	0.772 (0.782)	Möbius aromatic
5	exptl	−[e] [2]	−	−	8.56 [2] 8.72 [6] 9.92 [2] 10.01 [2]	−1.2 [21] −1.67 [18] −2.63 [3]			aromatic
	calcd	−1.9 [1] −2.0 [1]	−	−	8.7 to 10.6 [12]	−0.30 to −5.9 [42]	−13.8	0.812	aromatic
6	exptl	26.96 [2] 27.32 [2]	−	−	3.19 to 3.74 [12]	3.26 [18] 3.46 [3] 4.34 [18] 5.33 [3]			antiaromatic
	calcd	34.7 to 38.9 [4]	−	−	0.74 to 2.5 [12]	2.6 to 14.2 [42]	18.7	0.636 (0.724)	antiaromatic

[a] In $CDCl_3$ (see ref 10). [b] NMR and NICS values were calculated at B3LYP/6-31G(d,p) level. [c] Optimized planar geometry. [d] Optimized twisted geometry. [e] No NMR peaks were observed because of spectral congestion. [f] Calculated at nonweighted centers in hexaphyrin macrocycles at zero height. See the SI for detailed descriptions and for NICS values at other points. [g] HOMA values using optimized geometries (values using X-ray crystallographic structures are given in parentheses).

the spectrally dispersed WLC probe pulses were monitored by miniature spectrograph (OceanOptics, USB2000+). To obtain the time-resolved transient absorption difference signal (ΔA) at a specific time, the pump pulses were chopped at 25 Hz and the absorption spectra intensities were saved alternately with and without pump pulses. Typically, samples were excited with 6000 pulses to obtain the TA spectra at a particular delay time. The polarization angle between the pump and probe beams was set at the magic angle (54.7°) in order to prevent polarization-dependent signals. The cross-correlation fwhm in the pump−probe experiments was less than 200 fs, and the chirp of the WLC probe pulses was measured to be 800 fs in the 400−800 nm region. To minimize the chirp, all-reflection optics in the probe beam path and a 2 mm path length in the quartz cell were used. After the fluorescence and TA experiments, we carefully checked the absorption spectra of each compound to avoid artifacts from degradation and photooxidation of the sample. HPLC-grade toluene was used as the solvent for all of the steady-state and time-resolved spectroscopic studies.

Computational Methods. Quantum-mechanical calculations were performed using the Gaussian03 program suite.[13] All of the calculations were carried out using density functional theory (DFT) with Becke's three-parameter hybrid exchange functional and the Lee−Yang−Parr correlation functional (B3LYP) and employing a 6-31G(d,p) basis set for all of the atoms. The X-ray crystallographic structures were used as initial geometries for geometry optimization. The calculated ^{1}H NMR and nucleus-independent chemical shift (NICS) values were obtained for all of the molecules via the gauge-independent atomic orbital (GIAO) method at the same computational level as for the optimization process using the optimized geometries without any modification. The centers of rings with zero height for NICS(0) values were designated at several centroids that corresponded to the nonweighted centers of the carbons and nitrogens in the hexaphyrin macrocycles [see Figures S2 and S3 in the Supporting Information (SI) for detailed descriptions]. In the calculation of ^{1}H NMR spectra, we used as an internal reference the average ^{1}H NMR chemical shift value of 31.75 ppm for tetramethylsilane (TMS) calculated at B3LYP/6-31G(d,p) level. To simulate the ground-state absorption spectra, we used time-dependent DFT (TD-DFT) calculations with the same functional and basis set as for the NMR calculations. All of the computational analyses were carried out including all the peripheral substituents, since substituent effects should not be negligible in porphyrin and expanded porphyrin systems.

III. Results

NMR Spectra. The molecular aromaticity can be experimentally quantified using NMR techniques. The observed peaks in the ^{1}H NMR spectra of **3**−**6** are listed in Table 1. In the case of rectangular ethynyl-TIPS-substituted [26]hexaphyrin **3**, the inner protons were observed at −1.92 (N−H) and −2.23 ppm (peripheral β-H) in the NMR spectrum, whereas the outer protons were found in the range 9.37−9.91 ppm (peripheral β-H). The difference between the chemical shifts of the inner and outer protons ($\Delta\delta$) was determined to be 12.1 ppm, which reflects a strong diatropic ring current indicating a highly aromatic nature for **3** (Table 1 and ref 10). Unexpectedly, rectangular [28]hexaphyrin **4**, which should be antiaromatic on the basis of Hückel's [4*n*] rule, does not show any paratropic ring current but instead exhibits a nearly aromatic nature with a relatively small difference between the chemical shifts for the peripheral β-H protons ($\Delta\delta \approx 6.0$ ppm). Similar magnetic behavior was also observed in all-*meso*-pentafluorophenyl-substituted [26]/[28]hexaphyrins **1** and **2**.[7a] On the basis of the temperature-dependent NMR spectra of **2**, it was suggested that at least two conformational isomers, such as planar Hückel antiaromatic and twisted Möbius aromatic ones, could exist in solution as a rapid interconversion equilibrium within the NMR time scale. In comparison with the rectangular hexaphyrins, the spectacles-shaped vinylene-bridged hexaphyrins **5** and **6** show

(13) Frisch, M. J.; et al. *Gaussian 03*, revision C.02; Gaussian, Inc.: Wallingford, CT, 2004.

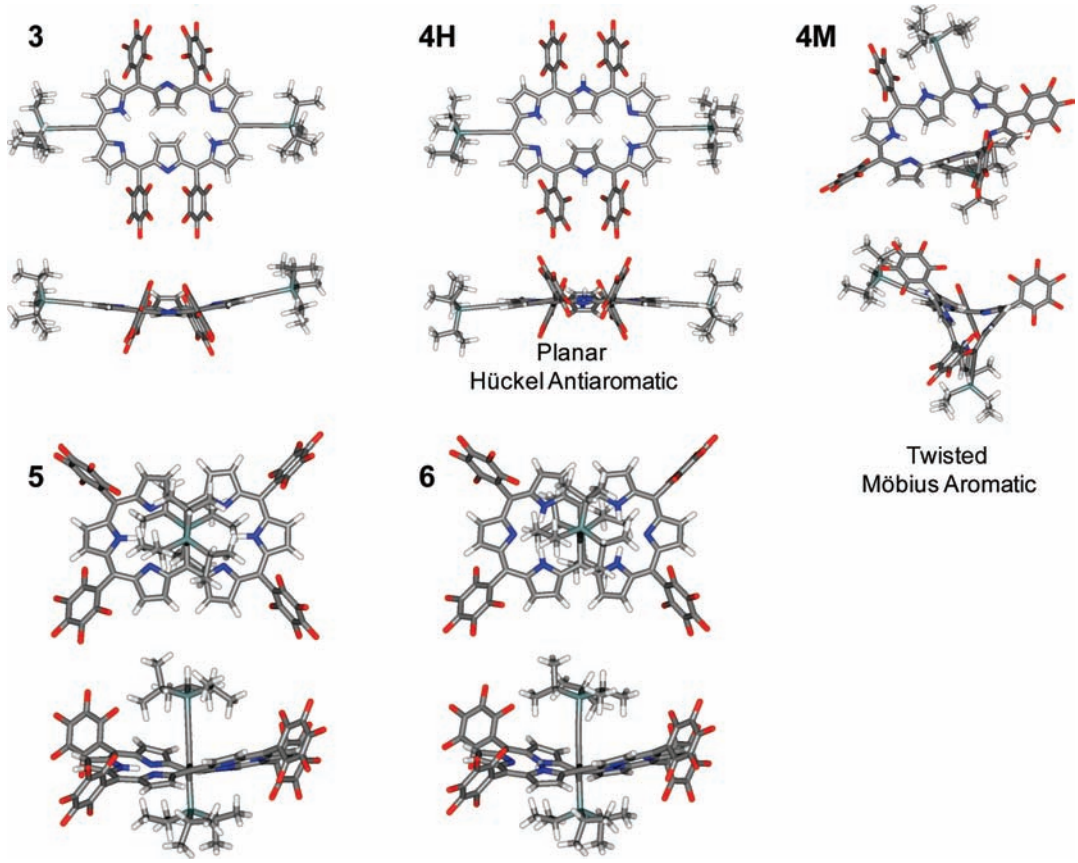

Figure 2. Optimized structures of **3**−**6** calculated at the B3LYP/6-31G(d,p) level. In the case of **4**, two different conformational isomers (**4H** and **4M**) were optimized individually from different initial geometries.

highly opposite magnetic properties. The outer peripheral β-protons were observed in the ranges 8.56−10.01 ppm for **5** and 3.19−3.74 ppm for **6**, indicating strong diatropic and paratropic ring currents, respectively, with Hückel topologies.

In order to determine the structures of conformational isomers of **4**, we simulated the ^{1}H NMR spectra using quantum-mechanical calculations, in which we used the optimized structures obtained from DFT calculations at the B3LYP/6-31G(d,p) level that employed X-ray crystallographic structures as initial geometries. The optimized structures of **3**−**6** depicted in Figure 2 are nearly the same as their X-ray crystallographic structures.[10] In the case of **4**, we proposed two representative conformational isomers with planar and twisted geometries (denoted here as **4H** and **4M**, respectively) because the preliminary X-ray crystallographic structure of **4** has a highly twisted conformation (Figure S1 in the SI). The calculated NMR peak positions for all of the protons in **3** are in good agreement with the experimental values (Table 1). In regard to the two optimized structures for **4**, the calculated chemical shift values for the twisted structure (**4M**) explained the experimental values well, indicating that most of the molecules seem to exist in the twisted conformation in solution. As shown in more twisted lemniscular figure-eight hexaphyrins, it is difficult to assign inner and outer protons at the curled positions.[14] Nevertheless, the positions of the observed ^{1}H NMR peaks of **4** are in accordance with the calculated values for the twisted structure **4M**. Furthermore, the calculated ^{1}H NMR data show that planar and twisted conformational isomers correspond to Hückel antiaromatic and Möbius aromatic structures, respectively. On the basis of these results, we can expect that rectangular [28]hexaphyrin **4**, like **2**, exists as a dynamic equilibrium between at least two stable conformational isomers, planar Hückel antiaromatic **4H** and twisted Möbius aromatic **4M**, with a predominant contribution by the latter.[7a] In line with this expectation, the Möbius-type twisted conformer of **4** was calculated to be 15.9 kcal/mol more stable than Hückel-type planar one at the B3LYP/6-31G(d,p) level. In the cases of **5** and **6**, the calculated ^{1}H NMR spectra are well-matched with the experimental spectra as a result of the structural resemblance between the optimized and X-ray structures.

Steady-State Absorption and Emission. The overall characteristics of the steady-state absorption and fluorescence spectra of **3** and **4** in toluene are similar to those of **1** and **2** in regard to their featured Soret- (B-) and Q-like absorption bands and strong NIR fluorescence, except for slight red shifts by ~40 nm due to elongation of the π-conjugation pathway along the two ethynyl-TIPS substituents (Figure 3a). It should be noted that the absorption spectrum of [28]hexaphyrin **4** does not resemble those of [4*n*]-antiaromatic expanded porphyrins based on Hückel topology, which have broad Soret bands and featureless, smeared Q-like bands without any fluorescence.[5,6,8] This feature supports the conclusion that **4** is not an antiaromatic species, as expected from the results found for the magnetic properties. On the other hand, the absorption and fluorescence spectra of **5** and **6** exhibit remarkable differences (Figure 3b). While the well-featured absorption and strong fluorescence spectra of Hückel-aromatic **5** are similar to those of **1** and **3**, the steady-state absorption and fluorescence spectra of **6** show

(14) (a) Rzepa, H. *Org. Lett.* **2008**, *10*, 949. (b) Allan, C. S. M.; Rzepa, H. S. *J. Org. Chem.* **2008**, *73*, 6615.

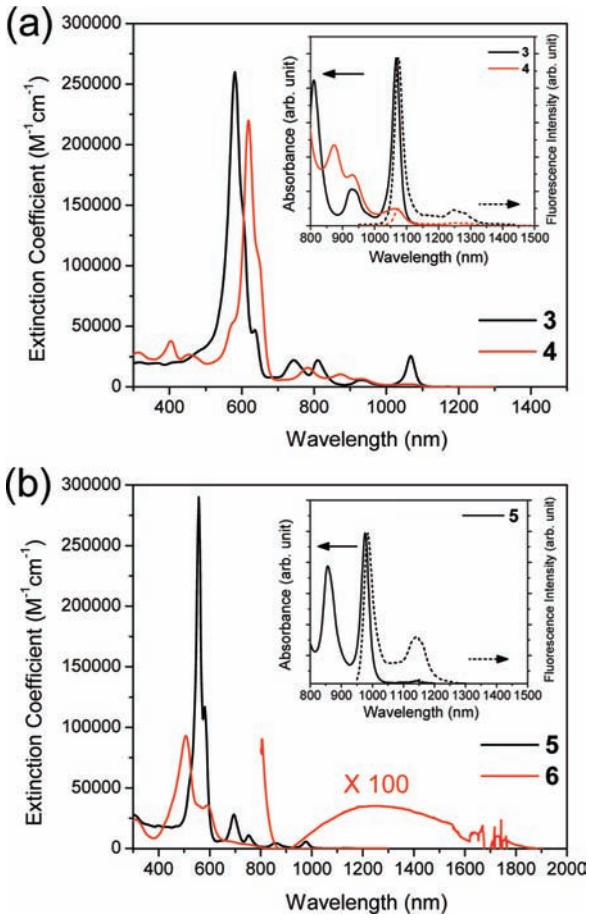

Figure 3. Absorption (solid lines) and fluorescence (dotted lines) spectra of **3**−**6** in toluene. The absorption band of **6** in the 900−1900 nm region is magnified for clarity. No emission signal was observed in the 800−2000 nm region for **6**.

unique features: (1) relatively broad and weak Soret-like bands located in the 400−600 nm region; (2) smeared Q-like bands in the 620−850 nm region; (3) an extremely weak and broad NIR absorption band in the 900−1800 nm region; and (4) a lack of fluorescence in the NIR region. These features have been frequently observed in other Hückel [4*n*]-antiaromatic porphyrin-related compounds.[5,6a,b,8] Phenylethynyl-substituted hexaphyrins **7** and **8** show steady-state photophysical properties similar to those of **5** and **6**, respectively (Figure S5 in the SI), indicating little difference between the TIPS and phenyl substituents with respect to their influence on the electronic structures of porphyrin macrocycles. A small Stokes shift of less than 200 cm^{-1} for **3**, **4**, **5**, and **7** suggests that structural changes in the excited and ground electronic states upon solvation are negligible.[15] All of the steady-state spectroscopic parameters are listed in Table 2.

Excited-State Dynamics. Femtosecond TA measurements were carried out to explore aromaticity-dependent excited-state photophysics. All of the TA spectra of **3**−**8** with photoexcitation of the Soret-like bands illustrate ordinary features seen in common porphyrinoids, such as strong ground-state bleaching (GSB) recovery in the Soret- and Q-like band regions and broad excited-state absorption (ESA) signals covering the whole visible region (Figure S6 in the SI). Figure 4 shows the temporal profiles at two representative wavelengths including GSB and

Table 2. Summary of Results from Steady-State and Time-Resolved Measurements on **3**−**8** in Toluene

sample	absorption λ_{max} (nm)	fluorescence λ_{max} (nm)[b]	ΔE_{Stokes} (cm^{-1})[d]	τ_{S_1} (ps)[e]
3	583, 745, 814, 934, 1067	1075, 1262	70	91.8 ± 2.9
4	624, 784, 871, 936, 1053	1074, 1265	186	124 ± 3
5	557, 694, 756, 858, 976	986, 1142	104	282 ± 5
6	507, 594, 660, 753, 1260[a]	−[c]	−[c]	8.6 ± 0.6
7	554, 690, 745, 854, 966	976, 1133	106	300 ± 4
8	510, 579, 675, 768, 1385[a]	−[c]	−[c]	13.1 ± 1.1

[a] Extremely weak bands with broad spectral widths. [b] Photoexcited at 442 nm. [c] Fluorescence was not detected. [d] Stokes shift. [e] Lifetime of the lowest singlet state (S_1).

ESA signals, respectively, retrieved from the TA spectra of **3**−**6** in toluene. Since the GSB and ESA signals for all of the molecules gave similar time constants from their decay profiles, we used averaged values as singlet-state lifetimes (Table S1 in the SI).[6,7] The temporal profiles of the femtosecond TA spectra of **3** and **4** show quite similar behavior. The lifetimes of the lowest singlet states of **3** and **4** were measured to be 92 ± 3 and 124 ± 3 ps, respectively, which are similar to those of **1** (98 ps) and **2** (115 ps) at room temperature,[7b] indicating that the effect of the ethynyl-TIPS substituent on the excited energy relaxation dynamics is negligible. On the other hand, in comparison with rectangular [26]hexaphyrins **1** and **3**, spectacles-shaped [26]hexaphyrin **5** shows a 3-fold longer S_1 state lifetime of 282 ± 5 ps, presumably because of the enhanced rigidity conferred by the internal vinylene bridge between the two meso carbons. Of interest here is the fact that antiaromatic **6** exhibits dramatically faster decay dynamics in the TA data. The temporal profiles of **6** and **8** can be fitted by a double-exponential decay function, giving rise to two time constants with values of <1 ps and ~10 ps. The former seems to represent the internal conversion time from the Q-like state to the lowest S_1 state (located at 1200−1600 nm), and the latter corresponds to the lifetime of the lowest S_1 state. The observed S_1 state lifetime of 8.6 ± 0.6 ps for **6** is 30 times shorter than that of the aromatic congener **5**. The phenylethynyl-substituted hexaphyrins **7** (300 ± 4 ps) and **8** (13.1 ± 1.1 ps) also show similar behaviors (Figures S7 and S8 in the SI). The shortened S_1 lifetimes of antiaromatic **6** and **8** are in accordance with their nonfluorescent properties, which arise from the acceleration of nonradiative internal conversion rates from the S_1 to the S_0 state due to the reduced energy gap between them.[15] It is noted that the intensities of the ESA signals in **6** and **8** are nearly comparable to those of the GSB signals, in constrast to normal aromatic porphyrins and expanded porphyrins, indicating that the relaxation of selection rules governed by the symmetry of electronic states is similar to that for antiaromatic porphyrins.[5b]

IV. Discussion

NICS and HOMA. It is now generally accepted that among various indices of aromaticity, the nucleus-independent chemical shift (NICS) value, which reflects magnetic shielding/deshielding by the induced π-electronic ring current, is one of the most appropriate methods for describing the aromatic nature of

(15) Turro, N. J. *Modern Molecular Photochemistry*; University Science Books: Sausalito, CA, 1991.

(16) (a) Schleyer, P. v. R.; Maerker, C.; Dransfeld, A.; Jiao, H.; Hommes, N. J. R. v. E. *J. Am. Chem. Soc.* **1996**, *118*, 6317. (b) Chen, Z.; Wannere, C. S.; Corminboeuf, C.; Puchta, R.; Schleyer, P. v. R. *Chem. Rev.* **2005**, *105*, 3842. (c) Cyrański, M. K.; Krygowski, T. M.; Wisiorowski, M.; Hommes, N. J. R. v. E.; Schleyer, P. v. R. *Angew. Chem., Int. Ed.* **1998**, *37*, 177.

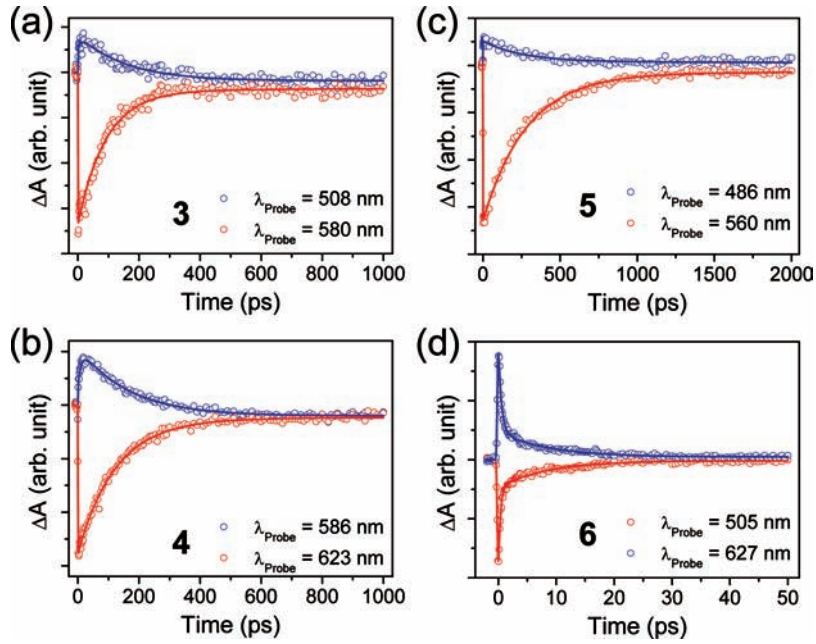

Figure 4. Temporal profiles of TA measurements on **3**−**6** in toluene. Data in blue and red show ESA and GSB signals, respectively.

π-conjugated cyclic molecular systems, such as expanded porphyrins.[3,6,7,16] For the quantitative evaluation of aromaticity, we calculated the NICS(0) values at several points within the molecular plane in the optimized geometries of relatively planar hexaphyrins except for **4M** (Figures S2 and S3 in the SI). Very recently, an approach for deciding meaningful ring centroids was applied using atoms-in-molecule (AIM) and electron localization function (ELF) critical point analyses.[14b] However, nonweighted centers for NICS(0) were used in this work because of their simple computational processes and comparatively reliable results.[16] Concurrent with Hückel's $[4n + 2]$ and $[4n]$ π electron rules on the π-conjugation pathways, the NICS(0) calculations show large negative and positive values, respectively, for the planar macrocycles (Table 1). Regardless of the molecular shape, the NICS(0) values of [26]hexaphyrins are large and negative (−15.0 ppm for **3** and −13.8 ppm for **5**), exhibiting efficient diatropic ring currents. On the other hand, [28]hexaphyrins have large, positive NICS(0) values of 35.2 and 18.7 ppm for planar **4H** and **6**, respectively. Especially, the twisted [28]hexaphyrin **4M** has a value of −13.0 ppm, in line with the expected Möbius aromatic nature. Because it is difficult to define the central points in distorted compounds such as **4M**, the NICS values for other positions were calculated and found to be in the range −10 to −15 ppm, thereby also representing the aromatic nature of **4M** (Figure S2). It should be noted that most of the NICS(0) values at noncentral points at a distance of ∼1 Å from adjacent C or N atoms are slightly larger than those at central positions for all of the compounds; these might be perturbed by local magnetic effects due to their proximity to the π-electronic conjugation pathway.[16c]

Another aromaticity index, the harmonic oscillator model of aromaticity (HOMA), which is based on the structural properties, can be a useful indicator of the quantification of aromaticity in heteroatom-containing systems such as porphyrinoids.[17] The HOMA value is given by eq 1:

$$\mathrm{HOMA} = 1 - \mathrm{EN} - \mathrm{GEO} \qquad (1)$$

where

$$\mathrm{EN} = \alpha(R_{\mathrm{opt}} - R_{\mathrm{av}})^2 \qquad (2)$$

and

$$\mathrm{GEO} = \frac{\alpha}{n}\sum_i (R_{\mathrm{av}} - R_i)^2 \qquad (3)$$

in which α is an empirical constant chosen to give HOMA = 0 for the hypothetical Kekulé structure and HOMA = 1 for the system with all bonds equal to the optimal bond length R_{opt}, n is the number of bonds in the summation, and R_{av} is the average of the R_i, where R_i is the heteroatom-corrected bond length of the ith bond in the π-conjugation pathway. The EN term (eq 2) describes changes in aromatic character due to a deviation of the average bond length from the optimal value, while the GEO term (eq 3) reflects the consequences of bond-length alternation. HOMA values were calculated along the π-conjugation pathways for all of the compounds **4**−**6** using their optimized structures (Table 1 and Figure S4 in the SI). Aromatic **3**, **4M** and **5** exhibit HOMA values of 0.7−0.8, whereas those of antiaromatic **4H** and **6** are ∼0.6. According to Herges' investigation of the relationship between the HOMA and NICS values in [16]annulene systems, opposite correlations were found for Möbius aromatic and Hückel antiaromatic compounds.[2c] As molecules become either more aromatic or more antiaromatic, their HOMA values increase more relative to those for nonaromatic systems, which is consistent with our results. This feature indicates that the π electrons are well-delocalized in all cases. Moreover, antiaromatic compounds have slightly smaller HOMA values than their aromatic congeners, because antiaromatic molecules tend to switch into nonaromatic ones via structural distortions, giving rise to an increase in the GEO term due to large bond-length alternation. For example, the GEO values of antiaromatic **4H** (0.1833) and **6** (0.2089) are much larger than those of aromatic **3** (0.0579), **4M** (0.0785), and **5** (0.0714) (Figure S4). The degree of bond-length alternation (Δr), which is directly related to the GEO term, shows a similar trend, with small Δr values (0.082−0.091 Å) for aromatic hexaphyrins and a large Δr value (0.11 Å) for antiaromatic ones.

(17) Krygowski, T. M.; Cyrański, M. K. *Chem. Rev.* **2001**, *101*, 1385.

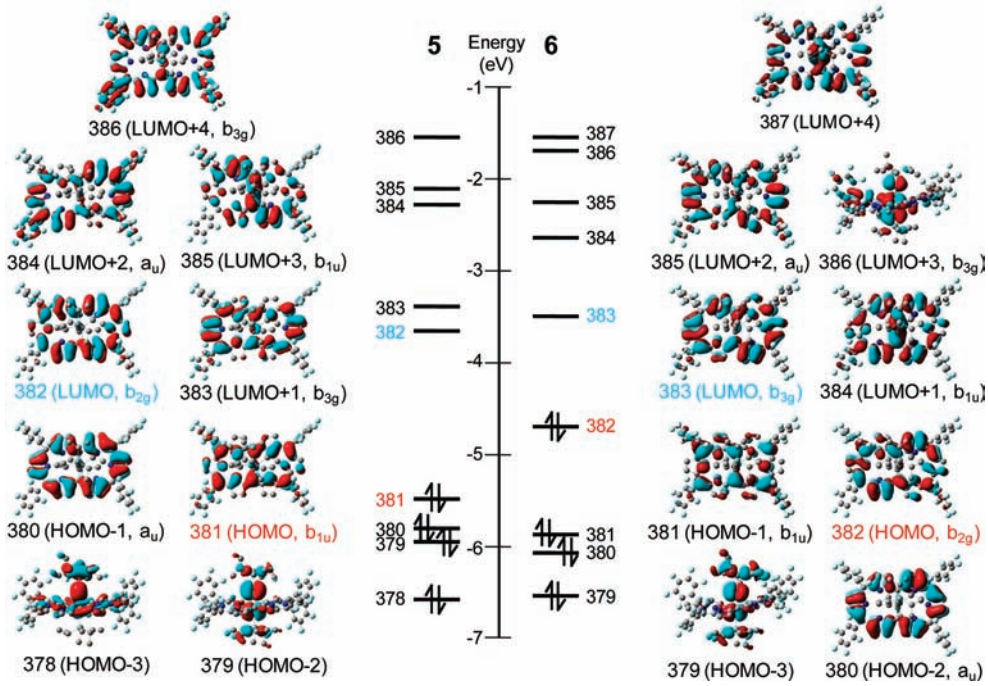

Figure 5. Frontier MOs of **5** and **6** calculated at B3LYP/6-31G(d,p) level.

As a consequence, we can conclude that rectangular [26]- and [28]hexaphyrins **1**−**4** are not ideally suited for a direct comparison of their photophysical properties in combination with the aromaticities determined by the number of π electrons ([4*n*] vs [4*n* + 2]) because of the conformational heterogeneity in 28 π-electron molecular systems.

Electronic Structures and Energy Relaxation Dynamics. In order to explain the distinct observation of a new NIR absorption band, a lack of fluorescence, a much reduced S_1 state lifetime, and an intensified ESA signal in Hückel antiaromatic molecular systems **6** and **8**, theoretical simulations such as frontier molecular orbital (MO) analyses and vertical excitation energy calculations would be quite relevant. For rectangular hexaphyrins **3** and **4** (both of which are planar, twisted conformers), the energies and orbital shapes of the MOs are similar to those of **1** and **2** (Figures S9 and S10 in the SI).[7] The relative energy of each MO is lower and some frontier MOs of **3** and **4** are more delocalized toward two ethyne bridges than are the corresponding ones in **1** and **2** because of the elongated π-conjugation pathway along the ethynyl-TIPS substituents, which is also responsible for a slight red-shift in the steady-state absorption and emission bands (Table 1). In this system, however, we should not directly compare their aromaticity-dependent nature with electronic structures, because **4** is not truly Hückel-antiaromatic, as mentioned earlier. Hence, here we will discuss in detail the MO structures of the vinylene-bridged systems **5** and **6**. Figure 5 presents the frontier MOs of **5** and **6** and their orbital energy levels. In spite of the different molecular shapes, the overall MO densities are similar to those of the rectangular hexaphyrins **1**−**4**, but new MOs localized on the vinylethynyl moieties were observed. As analogous to typical meso-aryl-substituted aromatic porphyrins,[18] spectacles-shaped hexaphyrin **5** has four frontier MOs: HOMO−1 (a_u, −5.64 eV), HOMO (b_{1u}, −5.40 eV), LUMO (b_{2g}, −3.53 eV), and LUMO+1 (b_{3g}, −3.33 eV), based on the D_{2h} point group. Interestingly, the frontier MOs of **6** are markedly different from those of **1**−**5**. First, the HOMO−LUMO energy gap in **6** is significantly reduced to 1.18 eV as compared with 1.87 eV in **5**. Second, the order and shape of each MO in **6** is similar to that in **5** except for the number of π electrons. The MO structure of **6** can be regarded simply as two π electrons added to an MO in **5**. It should be noted that 378th and 379th MOs for **5** and 379th and 386th MOs for **6** are mainly localized on internal vinyl-ethynyl conjugates whose orientations are perpendicular to π MOs of the macrocycles, indicating that the π conjugation in the hexaphyrin skeleton is not very significantly perturbed by the vinylene bridges or ethynyl substituents in vinylene-bridged hexaphyrins **5**−**8**.

Vertical excitation energies were calculated using time-dependent DFT (TD-DFT) to simulate the ground-state absorption spectra (Figure 6). In all cases, the calculated transitions are fairly well matched with the experimental absorption spectra with respect to both position and relative intensity. In the case of **5**, the simulated absorption spectrum can be simply explained by Gouterman's four-orbital model,[18] in which configuration interaction between four frontier MOs gives rise to two Soret-like and two Q-like bands, with weak intramolecular charge transfer (CT) bands between B- and Q-like bands contributed by the vinylethynyl conjugate (Table S2 in the SI). On the contrary, the calculated transitions of **6** (Figure 6b) are complicated and unusual in comparison with those of **3**−**5** (Figure S11 in the SI). The lowest singlet state was found at 1995 nm with an extremely small oscillator strength of 0.0019, indicating a one-photon optically forbidden state accessed by a direct HOMO−LUMO ($b_{3g} \leftarrow b_{2g}$) transition since one-photon g ← g transitions are generally forbidden (Table S3 in the SI).[5,15] Nevertheless, nonzero intensity may be due to symmetry lowering by the slightly ruffled structure of **6** (Figure 2). The observed broad and weak absorption band of **6** at ~1260 nm in the NIR region (inset of Figure 6b) may correspond to this optically dark state. In comparison with **5**, other bands appearing

(18) Gouterman, M. In *The Porphyrins*; Dolphin, D., Ed.; Academic Press: New York, 1978; Vol. III, Part A, pp 1−165.

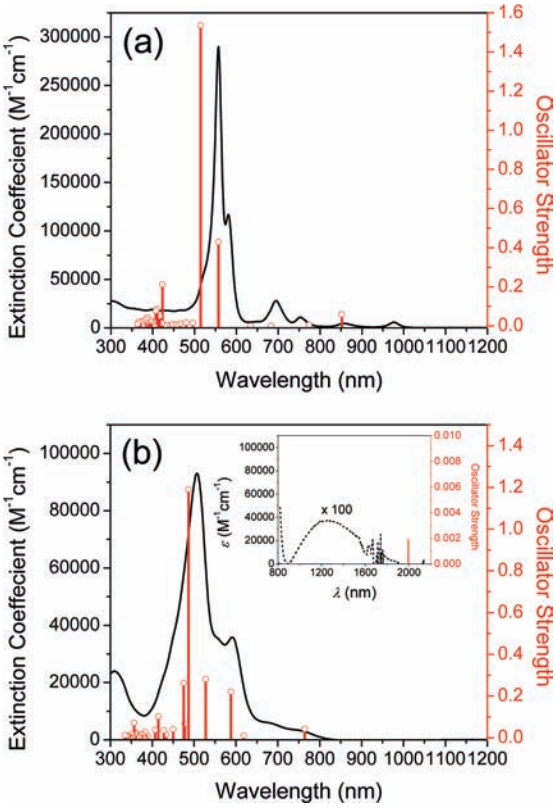

Figure 6. Vertical excitation energy data calculated using TD-DFT (red) compared with ground-state absorption spectra (black) for (a) **5** and (b) **6**.

in the visible region (except for CT transitions) are contributed by transitions from HOMO−2 to LUMO+2. Despite the similarity between the experimental and calculated absorption spectra, the fact that all of the bands in **6** are broader than those of the aromatic congener **5** cannot be simply explained at the present time. From these calculations, at least four and six frontier MOs should be considered in describing the absorption spectra of **5** and **6**, respectively, in the entire vis−NIR region.[3d]

According to the results from the TA spectra and ab initio calculations, the energy relaxation pathways in aromatic **5** and antiaromatic **6** can be suggested as shown in Figure 7. After photoexcitation to the Soret-like state (S_B) in **5**, the excited-state population relaxes efficiently to the lowest Q-like state (S_Q) in a shorter time than our temporal resolution of <200 fs and then decays to the ground state (S_0) within ∼300 ps. In the case of **6**, the S_Q state is depopulated within 1 ps to the optically dark S_1 state located at ∼1260 nm (0.98 eV), which can act as a ladder state in the energy relaxation process. This new optically dark state, which has rarely been reported in porphyrinoids, gives a dramatically shorter excited-state lifetime of 8.6 ps, mainly by means of the enhanced internal conversion rate (k_{IC}) obeying the energy-gap law given by the following equation:[5,15]

$$k_{IC} \approx 10^{13}\, e^{-\alpha \Delta E}$$

where α is a proportionality constant and Δ*E* is the HOMO−LUMO energy gap. We suggest that antiaromatic porphyrins and

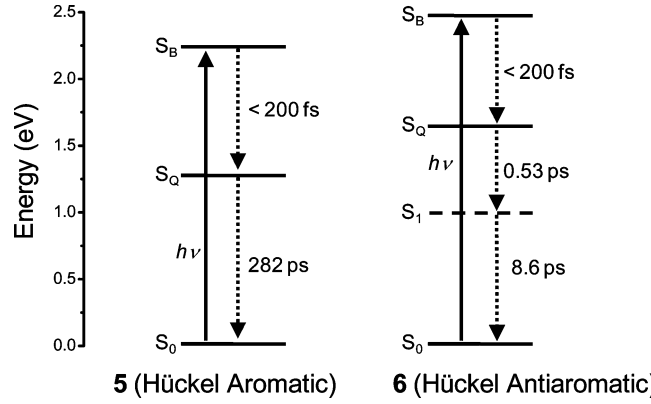

Figure 7. Schemes showing excited energy relaxation pathways for **5** and **6**. The dashed horizontal line corresponds to the one-photon optically forbidden singlet state. The energies measured by absorption spectra were used.

expanded porphyrins have much reduced HOMO−LUMO energy gaps with the same symmetry, giving rise to much weaker and lower-energy dark states that leading to shorter excited-state lifetimes than in their aromatic congeners.

V. Conclusions

In summary, the magnetic and structural characteristics of vinylene-bridged [26]- and [28]hexaphyrins exhibit Hückel aromatic and antiaromatic natures, respectively. The antiaromatic hexaphyrins **6** and **8** show broad, featureless absorption spectra, an optically dark NIR absorption band, a lack of fluorescence, and short lowest-excited-state lifetimes, which contrast sharply with the behavior of their aromatic congeners **5** and **7**. Overall, the photophysical properties of antiaromatic hexaphyrins arise from their unusual frontier MOs. Their short excited-state lifetimes originate from the one-photon-forbidden NIR state and should be a consequence of accelerated S_1-S_0 internal conversion due to the reduced HOMO−LUMO energy gap. Our results demonstrate that a difference in the electronic structures defined by aromaticity/antiaromaticity in [26]- and [28]hexaphyrins gives rise to a large change in their photophysical properties.

Acknowledgment. This work was supported by the Star Faculty and World Class University (2008-8-1955) Programs of the Ministry of Education, Science and Technology of Korea and AFSOR/AOARD Grant FA4869-08-1-4097 (D.K.). M.C.Y. and S.C. are thankful for the fellowship from the BK 21 Program of the Ministry of Education, Science and Technology. The quantum calculations were performed using the supercomputing resources of the Korea Institute of Science and Technology Information (KISTI). The work at Kyoto University was financially supported by a Grant-in-Aid for Scientific Research from MEXT (19205006).

Supporting Information Available: X-ray structure and crystallographic data (CIF) for **4**, complete refs 7a and 13, spectroscopic data for **7** and **8**, and results of quantum-mechanical calculations on **3**−**6**. This material is available free of charge via the Internet at http://pubs.acs.org.

JA9000536